Research Article Vol. 38, No. 9 / September 2021 / Journal of the Optical Society of America B C63

Journal of the Optical Society of America B

OPTICAL PHYSICS

Entangled two-photon absorption spectroscopy with varying pump wavelengths

LUTZ MERTENSKÖTTER,[1,2,*] KURT BUSCH,[1,3] AND ROBERTO DE J. LEÓN-MONTIEL[4]

[1]Humboldt-Universität zu Berlin, Institut für Physik, AG Theoretische Optik & Photonik, D-12489 Berlin, Germany
[2]Weierstrass Institute for Applied Analysis and Stochastics, Mohrenstraße 39, 10117 Berlin, Germany
[3]Max-Born-Institut, Max-Born-Straße 2A, 12489 Berlin, Germany
[4]Instituto de Ciencias Nucleares, Universidad Nacional Autónoma de México, Apartado Postal 70-543, 04510 Cd. Mx., Mexico
*Corresponding author: mertenskoetter@wias-berlin.de

Received 21 April 2021; revised 14 June 2021; accepted 14 June 2021; posted 17 June 2021 (Doc. ID 428531); published 14 July 2021

In entangled two-photon absorption (eTPA) spectroscopy, information about the energy-level structure of an arbitrary sample is retrieved by Fourier transforming sets of measured two-photon absorption probabilities of entangled photon pairs where the degree of entanglement and the delay time between the photons are varied. This works well for simple systems but quickly becomes rather difficult when many intermediate states are involved. We propose and discuss an extension of eTPA spectroscopy that solves this problem by means of repeated measurements at different pump wavelengths, thus reducing the experimental complexity of eTPA spectroscopy by removing the need to control the correlations of the entangled photons. Specifically, we demonstrate that our extension works well for a variety of realistic experimental setups.

https://doi.org/10.1364/JOSAB.428531

1. INTRODUCTION

Today, there exists a great variety of spectroscopic techniques—each with its own set of advantages and disadvantages—for myriad applications ranging from medicine [1] and material science [2] to biology [3], etc. Some of the more sophisticated protocols that have emerged are related to two-photon spectroscopic techniques, where two timed photon pulses interact with the sample in short succession. Specifically, entangled two-photon absorption (eTPA) spectroscopy [4–20] represents a technique that utilizes the quantum nature of light to devise a powerful spectroscopic tool. Although there is a current debate on the true quantum enhancement that such a technique might offer [21–23], an experimental demonstration of its working principle—namely, entangled-photon absorption—has become a topic of lively interest very recently [24–28]. Interestingly, eTPA has been applied to propose novel experimental schemes that might be used for determination of the electronic level structure of single molecules [5] and complex light-harvesting systems [29,30], and has become a useful addition to the spectroscopic toolbox. In fact, eTPA spectroscopy as originally proposed by Saleh *et al.* in 1998 [4] relies on tuning and integrating over the entanglement time T_e (a parameter of the second-order quantum correlation of the photon pair; see Section 2) to separate those features of the spectrum that allow direct access to the eigenenergies of the material from spurious background signals. However, this method can quickly become quite involved, as it requires multiple experiments with two-photon states that bear different temporal correlations. Consequently, novel ways of extracting information from eTPA signals have to be considered [19].

In this work, we develop a variant of this technique by exploiting the eTPA signal's dependence on the wavelength of the pump light. More specifically, our proposed scheme extracts information about the electronic level structure of the samples under study by correlating measurements at two or more different pump wavelengths. Our setup could be realized using standard and widely used entangled-photon sources, thus opening up a novel avenue towards nonlinear quantum spectroscopy.

Our work is organized as follows. In Section 2, we describe the model setup and basic workings of ordinary eTPA spectroscopy, and elucidate the problem of many intermediate states. We introduce our extension of eTPA spectroscopy to multiple pump wavelengths in Section 3 and provide a detailed discussion of its applicability in realistic settings. Finally, we summarize our findings and conclude in Section 4.

2. MODEL

Our model setup consists of a source of entangled photon pairs with tunable delay for two-photon absorption spectroscopy, a multi-level material system, and a second-order perturbative analysis of the eTPA signals.

We consider an entangled-photon spectroscopy setup as schematically depicted in Fig. 1. The light source we employ is a two-photon state created by collinear type-II spontaneous parametric downconversion (SPDC) with a continuous-wave pump and

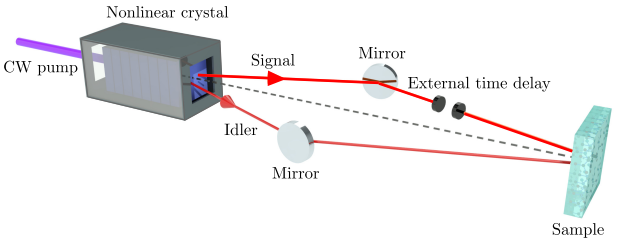

Fig. 1. Schematic of eTPA spectroscopic setup. A collinear type-II SPDC source is pumped with monochromatic light of angular frequency ω_p and produces two entangled photons with the frequencies ω_s and ω_i with a common central angular frequency $\omega_0 = \omega_p/2$. A tunable delay τ is introduced into the path of one of the photons. Subsequently, both photons interact with a material system whose electronic level structure is schematically depicted in Fig. 2.

is described by the spectral decomposition

$$|\psi^F\rangle = \int_{-\infty}^{\infty}\int_{-\infty}^{\infty} \mathrm{d}\omega_s\,\mathrm{d}\omega_i\,\Phi(\omega_s,\omega_i)\hat{a}^\dagger_{\omega_s}\hat{a}^\dagger_{\omega_i}|0\rangle, \tag{1}$$

with $\hat{a}^\dagger_{\omega_s}$, $\hat{a}^\dagger_{\omega_i}$ being the creation operators for the signal (s) and idler (i) photons, respectively. The joint spectral function of the photons is given by

$$\Phi(\omega_s,\omega_i) = \left(\frac{T_e}{\sqrt{\pi}}\right)^{1/2}\delta(\omega_p-(\omega_s+\omega_i))\mathrm{sinc}\left(\frac{T_e}{2}(\omega_s-\omega_i)\right)e^{i\omega_s\tau}, \tag{2}$$

which is commonly referred to as the twin state [31]. Here, l denotes the path length within the birefringent nonlinear crystal, ω_p is the angular frequency of the (monochromatic) light used to pump the SPDC source, ω_s and ω_i are the angular frequency of the signal and idler downconverted photons, respectively, and τ is the external delay introduced into the path of the signal photon. Furthermore, the entanglement time T_e is

$$T_e = l(N_s - N_i)/2, \tag{3}$$

with the inverse group velocities $N_s = 1/v_{g,s}$ ($N_i = 1/v_{g,i}$) of the signal (idler) photons. Note that in the analysis below, we will assume that the photons are degenerate with central wave-packet frequencies $\omega_s^0, \omega_i^0 = \omega_0 = \omega_p/2$.

The sample material model is a multi-level system with non-degenerate energy eigenstates $|j\rangle$ with respective energies $\hbar\epsilon_j$ (see Fig. 2). It is described by the Hamiltonian

$$\hat{H}_0 = \sum_j \hbar\epsilon_j|j\rangle\langle j|. \tag{4}$$

Two of these states fulfill the two-photon resonance condition

$$\epsilon_f - \epsilon_i = 2\omega_0 = \omega_p, \tag{5}$$

and we consider them as the initial state $|i\rangle$ and the final state $|f\rangle$. The final state is assumed to lie within a band of closely spaced levels. It is important to note that in any realization of our setup, $|f\rangle$ is defined by our choice of ω_p. The remaining N states are intermediate states that contribute as pathways to the two-photon absorption signal, i.e., the eTPA probability. These intermediate states are virtual states in the sense that they are energy eigenstates states ϵ_j of the unperturbed system, whose

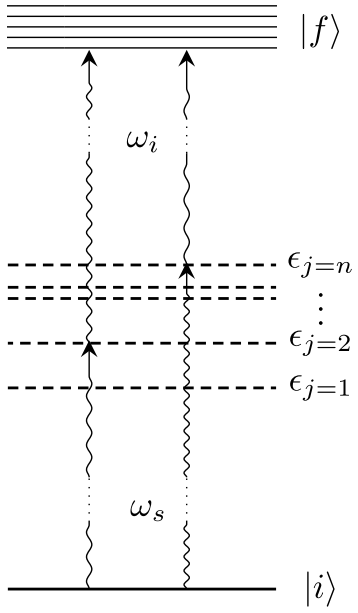

Fig. 2. Multi-level system including a number of intermediate states with energies ϵ_j and a band of final states $|f\rangle$. The entangled photons are frequency-anti-correlated and satisfy $\omega_s + \omega_i = \epsilon_f - \epsilon_i$. The arrows indicate two possible transition pathways mediated by different intermediate states.

detuning to the center frequencies ω_0 of the entangled photons is larger than two times the Rabi frequency [32].

Using second-order perturbation theory, we can calculate the two-photon transition probabilities $\mathcal{P}_{fi}$ from the initial to the final state upon interaction with the twin field state. Within dipole- and rotating-wave approximation, the perturbation, i.e., the interaction Hamiltonian, is described in the interaction picture as

$$\hat{V}(t) = \hat{\mu}(t)\hat{E}^+(t) = \left(\frac{\hbar\omega_0}{4\pi\epsilon_0 c A}\right)^{1/2}\int_{-\infty}^{\infty}\mathrm{d}\omega\hat{\mu}(t)\hat{a}_\omega(t) + \mathrm{H.c.}, \tag{6}$$

where $\hat{\mu}(t)$ denotes the dipole operator.

Through a Fourier transform in conjunction with suitable coordinate transformations, the time-ordered time integral that arises in second-order perturbation theory evaluates to [19]

$$\mathcal{P}_{fi} = \left(\frac{\omega_p^2}{4\hbar^2\sqrt{\pi}\epsilon_0^2 A^2 T_e}\right)2\pi t\delta^{(t)}(\epsilon_f-\epsilon_i-\omega_p)s(T_e,\tau), \tag{7}$$

with the delta-like function of width $4/\pi t$:

$$\delta^{(t)}(\epsilon_f-\epsilon_i-\omega_p) = \frac{2\sin^2((\epsilon_f-\epsilon_i-\omega_p)t/2)}{\pi t(\epsilon_f-\epsilon_i-\omega_p)^2}, \tag{8}$$

and

$$s(T_e,\tau) = \left|\sum_j A_j(2 - e^{-i\Delta_j(T_e+\tau)} - e^{-i\Delta_j(T_e-\tau)})\right|^2. \tag{9}$$

In these expressions, we denote the energy mismatch of the center frequencies of the entangled photons ω_0, the intermediate states by $\Delta_j = \epsilon_j - \epsilon_i - \omega_0$, and the transition matrix elements are $A_j = \mu_{fj}\mu_{ji}/\Delta_j$, where $\mu_{kl} = \langle k|\hat{\mu}|l\rangle$ are the corresponding transition dipole moments. The delta-like function ensures energy conservation for times large compared to the energy mismatch of the pump angular frequency and the energy of the total transition.

Expanding the absorption cross section $s(T_e, \tau)$ now gives us

$$s(T_e,\tau) = \sum_{j,k} A_j A_k^* \left(4 - [e^{i\Delta_j - \Delta_k \tau} + \text{c.c.}] - 2e^{-i\Delta_j T_e}[e^{i\Delta_j \tau} + \text{c.c.}] - 2e^{\Delta_k T_e}[e^{i\Delta_k \tau} + \text{c.c.}] - e^{-(\Delta_j - \Delta_k T_e)}[e^{i\Delta_j + \Delta_k \tau} + \text{c.c.}]\right). \tag{10}$$

Note that for N intermediate states ϵ_j, the Fourier transform with respect to τ, i.e., the eTPA spectrum, shows peaks at zero angular frequency, as well as the $2(N+1)N$ angular frequencies

$$\pm\Delta_j = \pm(\epsilon_j - \omega_0), \tag{11}$$

$$\pm(\Delta_j - \Delta_k) = \pm(\epsilon_j - \epsilon_k), \tag{12}$$

$$\pm(\Delta_j + \Delta_k) = \pm(\epsilon_j + \epsilon_k - 2\omega_0), \tag{13}$$

where ϵ_j, ϵ_k denote the energies of the intermediate states. To illustrate how the different frequency peaks appear in the Fourier transform of the eTPA signal, we display in Fig. 3(a) a system with two randomly selected intermediate states for a fixed value of the pump wavelength of $\lambda_p = 405$ nm, corresponding to a central angular frequency of the entangled photons of $\omega_0 = c\pi/\lambda_p = 1.53$ eV. For simplicity, all dipole moments have been set to the same constant value for all transitions.

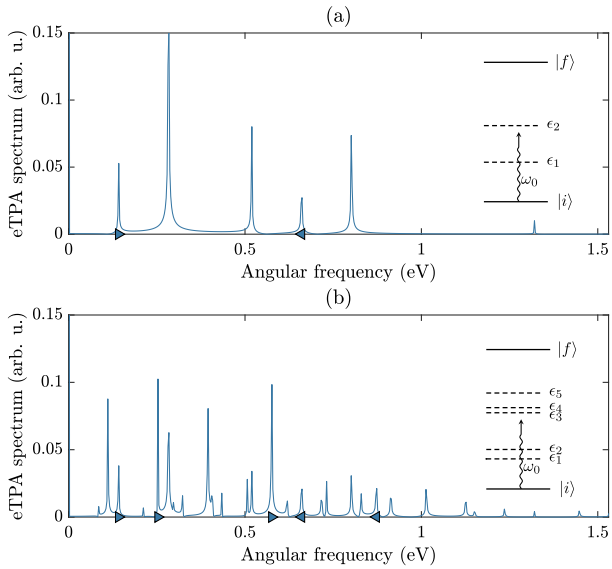

Fig. 3. Spectrum of the eTPA signal showing the angular frequency of oscillations of the absorption cross section [Eq. (10)] for two different matter systems with (a) two intermediate states at $\epsilon_1 = 0.86$ eV and $\epsilon_2 = 1.67$ eV and (b) five intermediate states at $\epsilon_1 = 0.66$ eV, $\epsilon_2 = 0.87$ eV, $\epsilon_3 = 1.67$ eV, $\epsilon_4 = 1.78$ eV, and $\epsilon_5 = 2.11$ eV. The energy mismatches $+\Delta_j$ $(-\Delta_j)$ are indicated by the right (left) facing triangles. Note that the number of peaks in the eTPA spectrum grows quadratically with the number of intermediate states. With a growing number of intermediate states, it quickly becomes difficult to deduce the underlying energy levels from such spectra.

We observe that even though the energy mismatch Δ_1 of the lower intermediate state is much larger than the energy mismatch Δ_2 of the higher intermediate states, the corresponding peaks of the spectrum (marked with triangles) do not differ proportionally in size. This suggests that, as a general rule, the heights of the peaks are not a reliable way of making sense of the spectrum and do not allow to deduce the underlying energy structure of the sample [4,7].

In Fig. 3(b), we infer that it quickly becomes difficult to interpret the spectrum when the number of intermediate states grows. This results from the fact that the number of spectral peaks grows quadratically with the number of immediate levels. Clearly, this severely limits the usefulness of the eTPA spectroscopy in the present form.

3. EXTRACTING ENERGIES OF INTERMEDIATE-STATE LEVELS

Our goal is to extract the energies of the intermediate states ϵ_j from the eTPA spectrum. An easy way to achieve this would be to identify within these peaks those at the frequencies Δ_j of Eq. (11), as these depend on only one of the eigenenergies ϵ_j, and its respective value is readily extracted by adding ω_0. For systems with a small number of intermediate states, it may also be feasible to find the correct values by guessing the N intermediate states as follows. First, we would guess the Δ_j and then plug them into Eqs. (11)–(13) and check whether the resulting frequencies line up with the actual spectrum. This approach can easily be carried out with simple spectra such as that in Fig. 3(a).

However, in the general situation, there are $2(N+1)N$ peaks, and for the aforementioned technique of "educated guessing," we would have to select N members from this set and check whether they align with the actual spectrum. Clearly, this scheme quickly becomes rather cumbersome to execute; see Fig. 3(b). Moreover, for systems with many intermediate states, another detrimental effect sets in and fundamentally obstructs the extraction of relevant information from a spectrum. Specifically, as the number N of peaks increases, it becomes more and more likely to encounter overlapping peaks with low amplitudes or very shallow signals that get lost in the background noise so that it will become less and less likely that the approach of educated guessing will succeed. The immediate response to this challenge would be to reduce the noise floor and to increase spectral resolution, but there clearly are limits to what reasonably can be done. In what follows, we, therefore, address this problem by extending eTPA spectroscopy by means of repeated measurements at different pump wavelengths.

A. Dependence of $s(T_e, \tau)$ on Pump Wavelength

Fortunately, the sets of frequencies in Eqs. (11)–(13) are set apart from all other frequencies by their dependence on ω_0 as demonstrated in Fig. 4. Most importantly, the locations of the $+\Delta_j$ signals in Eq. (11) go with $-\omega_0$. This

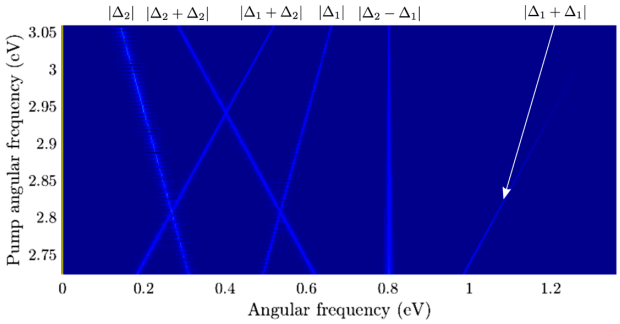

Fig. 4. Spectrum of the eTPA signal at a range of different pump frequencies starting at $\omega_p = 2\omega_0$, i.e., the top edge of the plot corresponds to Fig. 3(a). At the top, the peaks are labeled in terms of the sets of frequencies in Eqs. (11)–(13). We observe that the three distinct slopes clearly identify each peak as a member of one of the three distinct sets.

implies that by measuring at different pump wavelengths, i.e., different single-photon, degenerate central frequencies $\omega_0 = \{\omega_0^1, \omega_0^2, \cdots, \omega_0^n\}$, with the nth pump frequency given by $\omega_p^n = 2\omega_0^n$, we will be able to uniquely identify the intermediate-state energies of the sample. Remarkably, as mentioned above, their behavior with ω_0 allows us to distinguish them from the peaks in Eq. (12), which do not depend on ω_0, and the peaks in Eq. (13), which change with $2\omega_0$.

In Fig. 5, we display the eTPA spectrum for the same two-intermediate-state samples as in Fig. 3(a), considering two different central frequencies of the pump. Note that in these plots, the peaks corresponding to the frequencies $+\Delta_j$ of the two spectra are separated by a distance $\pm(\omega_0^1 - \omega_0^2)$. Now, we simply run a signal processing routine to identify the set of peaks of both spectra and find pairs, one element from each spectrum, that are separated by $\pm(\omega_0^1 - \omega_0^2)$. By adding the respective ω_0 to these peaks, we can thus find the intermediate states $\epsilon_j = \Delta_j + \omega_0$. This process can easily be automated.

An important advantage of this technique is that we can make further measurements at additional pump wavelengths should two measurements be insufficient to deduce the ϵ_j from the spectrum. This is preferable over simply increasing the resolution in the delay time τ and decreasing statistical errors through repeated measurements of the same system, as features of the spectrum that are obscured by the overlapping of the peaks

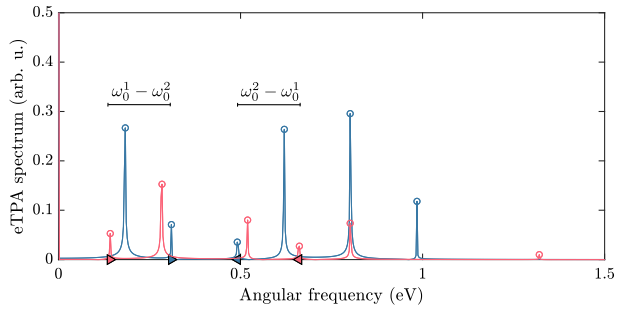

Fig. 5. Spectrum of the eTPA signal at $\omega_0^1 = 1.53$ eV (blue) and $\omega_0^2 = 1.36$ eV (red). The circles represent the peaks identified by our signal processing routine. The energy mismatches $+\Delta_j$ ($-\Delta_j$) are indicated by the right (left) facing triangles. Note that exactly two pairs of peaks from the different spectra are separated by $\pm(\omega_0^1 - \omega_0^2)$, allowing us to identify the two intermediate-state energies ϵ_j.

or low peak amplitudes at a particular frequency tend not to overlap or to be poorly visible at another pump frequency. This is due to the fact that peak positions and amplitudes also change with the pump frequency.

B. Discrete Fourier Transform and Experimental Accessibility of Our Technique

While the basic scheme laid out here is rather simple, a number of potential problems lie in the choice of parameters for the experiment. In an actual experiment, the values of τ are discrete. Assuming a free delay line with a mirror setup on a translation stage, their spacing Δ_τ is determined by the smallest path delay we can introduce. Here, we are using a value of $\Delta_\tau = 0.3 \times 10^{-15}$ s, which, using a mirror, translates to a step size $\Delta_L = c\Delta_\tau/2 = 45$ nm, which is attainable using modern translation stages [33].

As we are using a discrete Fourier transform, our angular frequency resolution ω_{res} is defined by our sampling rate in time, i.e., smallest path delay, Δ_τ and the number of points we can measure $\tau_N = \tau_{\max} - \tau_{\min}/\Delta_\tau$ by

$$\omega_{\text{res}} = \frac{\Delta_\tau}{\tau_N} = \frac{1}{\tau_{\max} - \tau_{\min}} > \frac{\Delta_\omega}{2\pi}. \tag{14}$$

The inequality follows from the fact that the range of τ we can access is, in turn, limited by the bandwidth Δ_ω of our entangled photons, as it defines their entanglement time T_e. Here, we assume an SPDC type-II source with a bandwidth of $\Delta_\omega = 7.4$ meV [34], resulting in an entanglement time of

$$T_e = \frac{\pi}{\Delta_\omega} \approx 1745 \text{ fs}. \tag{15}$$

The two photons have to overlap in space–time to contribute to two-photon absorption, and thus we have

$$\tau_{\max} = -\tau_{\min} < T_e. \tag{16}$$

Furthermore, peaks that are supposed to be measurable with a simple setup need to lie roughly within the bandwidth Δ_ω of our photons. This is a serious constraint, as at the same time, our angular frequency resolution ω_{res} becomes poorer for large bandwidth and, consequently, small entanglement times T_e [see Eq. (14)]. In other words, ideally, we would want a large Δ_ω and a small ω_{res}, which by (14) is mutually exclusive. In Fig. 6, we illustrate this effect for two choices of Δ_ω.

This problem could be addressed by increasing the photon flux to offset the limited bandwidth and increase visibility of otherwise very low peaks. However, when choosing a bright source, we must take care to not exceed intensities Φ for which the quantum processes still cease to dominate the absorption rate [31]. Specifically, the absorption cross section R has two contributions:

$$R = R_e + R_r = \sigma_e \Phi + \delta_r \Phi^2, \tag{17}$$

where δ_r is the classical, i.e., probabilistic, absorption cross section, and $\sigma_e \propto \mathcal{P}_{fi}$ is the quantum–mechanical cross section. It is the latter that we are trying to measure. Their actual values depend on the experiment and have been analyzed in detail in Refs. [4,21,22].

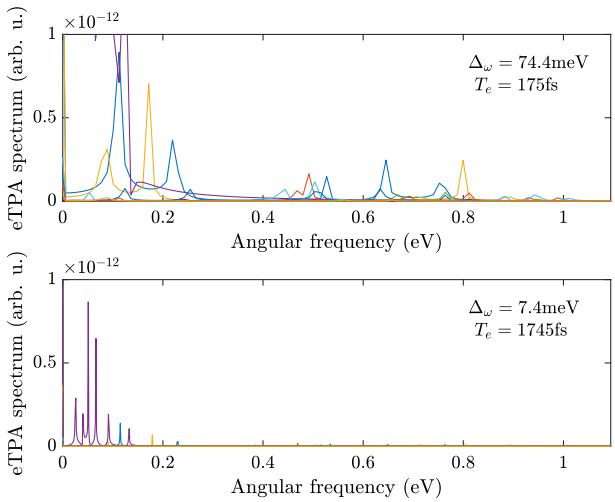

Fig. 6. eTPA spectra for 10 random sets of two intermediate states each for two different choices of Δ_ω (T_e) at constant $\Delta_L = 45$ nm and pump wavelength $\lambda_p = 405$ nm. We observe that a small bandwidth leads to strong attenuation of peaks at frequencies far from the resonance (bottom), yet a large bandwidth results in poor resolution in ω (top).

Finally, it is worth remarking that the angular frequency range of the eTPA spectrum is determined by our sampling rate in time as

$$\omega_{\max} = \frac{2\pi}{2\Delta_\tau} = -\omega_{\min} \tag{18}$$

and does not tend to be a limiting factor on our choice of parameters.

4. CONCLUSION

We have demonstrated that the pump frequency ω_p of a type-II SPDC source represents an additional resource for eTPA spectroscopy. Specifically, we have shown that a varying pump wavelength provides a robust way to interpret the spectroscopic data that otherwise may well be very difficult to interpret. In particular, for samples with complex energy spectra and when many intermediate states contribute to the two-photon absorption, our novel approach can make eTPA spectroscopy feasible. Further, our analyses of the limitations in the choice of parameters have revealed that there is ample room for balanced choices regarding frequency resolution as well as the frequency range. How these are weighted depends on the concrete problem at hand. Further, the trade-off between resolution and range can, to some extent, be relaxed by reducing the step size Δ_L using more sophisticated delay lines.

Funding. Deutsche Forschungsgemeinschaft (EXC-2046/1, project ID: 390685689, Project 182087777); Dirección General de Asuntos del Personal Académico, Universidad Nacional Autónoma de México (UNAM-PAPIIT IN102920); Consejo Nacional de Ciencia y Tecnología (CB-2016-01/284372).

Acknowledgment. We thank Armando Perez-Leija for many fruitful discussions on the topic, as well Sven Ramelow for his valuable insights on the experimental side of things. R. J. L.-M. thankfully acknowledges financial support by CONACyT under the project CB-2016-01/284372 and by DGAPA-UNAM under the project UNAM-PAPIIT IN102920; L. M. acknowledges funding by the Deutsche Forschungsgemeinschaft (DFG, German Research Foundation) under Germany's Excellence Strategy – The Berlin Mathematics Research Center MATH+ (EXC-2046/1, project ID: 390685689); K. B. and R. J. L.-M. acknowledge financial support by the Deutsche Forschungsgemeinschaft (DFG), SFB 951 (Project 182087777).

Disclosures. The authors declare no conflicts of interest.

Data Availability. Data underlying the results presented in this paper are not publicly available at this time but may be obtained from the authors upon reasonable request.

REFERENCES

1. J. Luypaert, D. Massart, and Y. V. Heyden, "Near-infrared spectroscopy applications in pharmaceutical analysis," Talanta **72**, 865–883 (2007).
2. I. Noda and Y. Ozaki, *Two-Dimensional Correlation Spectroscopy: Applications in Vibrational and Optical Spectroscopy* (Wiley, 2005).
3. A. Tu, *Raman Spectroscopy in Biology, Principles and Applications* (Wiley, 1982).
4. B. E. A. Saleh, B. M. Jost, H.-B. Fei, and M. C. Teich, "Entangled-photon virtual-state spectroscopy," Phys. Rev. Lett. **80**, 3483–3486 (1998).
5. J. Kojima and Q.-V. Nguyen, "Entangled biphoton virtual-state spectroscopy of the A-X system of OH," Chem. Phys. Lett. **396**, 323–328 (2004).
6. J. Peřina, B. E. A. Saleh, and M. C. Teich, "Multiphoton absorption cross section and virtual-state spectroscopy for the entangled n-photon state," Phys. Rev. A **57**, 3972–3986 (1998).
7. R. de J. León-Montiel, J. Svozilík, L. J. Salazar-Serrano, and J. P. Torres, "Role of the spectral shape of quantum correlations in two-photon virtual-state spectroscopy," New J. Phys. **15**, 053023 (2013).
8. K. E. Dorfman, F. Schlawin, and S. Mukamel, "Nonlinear optical signals and spectroscopy with quantum light," Rev. Mod. Phys. **88**, 045008 (2016).
9. F. Schlawin, "Tutorial—entangled photon spectroscopy," J. Phys. B **50**, 203001 (2017).
10. H. Oka, "Efficient selective two-photon excitation by tailored quantum-correlated photons," Phys. Rev. A **81**, 063819 (2010).
11. F. Schlawin, K. E. Dorfman, and S. Mukamel, "Entangled two-photon absorption spectroscopy," Acc. Chem. Res. **51**, 2207–2214 (2018).
12. J. P. Villabona-Monsalve, O. Calderón-Losada, M. Nuñez Portela, and A. Valencia, "Entangled two photon absorption cross section on the 808 nm region for the common dyes zinc tetraphenylporphyrin and rhodamine B," J. Phys. Chem. A **121**, 7869–7875 (2017).
13. O. Varnavski, B. Pinsky, and T. Goodson, "Entangled photon excited fluorescence in organic materials: an ultrafast coincidence detector," J. Phys. Chem. Lett. **8**, 388–393 (2017).
14. H. Oka, "Enhanced vibrational-mode-selective two-step excitation using ultrabroadband frequency-entangled photons," Phys. Rev. A **97**, 063859 (2018).
15. H. Oka, "Two-photon absorption by spectrally shaped entangled photons," Phys. Rev. A **97**, 033814 (2018).
16. J. Svozilík, J. Peřina, and R. de J. León-Montiel, "Virtual-state spectroscopy with frequency-tailored intense entangled beams," J. Opt. Soc. Am. B **35**, 460–467 (2018).
17. J. Svozilík, J. Peřina, and R. de J. León-Montiel, "Two-photon absorption spectroscopy using intense phase-chirped entangled beams," Chem. Phys. **510**, 54–59 (2018).
18. R. K. Burdick, O. Varnavski, A. Molina, L. Upton, P. Zimmerman, and T. Goodson, "Predicting and controlling entangled two-photon absorption in diatomic molecules," J. Phys. Chem. A **122**, 8198–8212 (2018).
19. R. de J. León-Montiel, J. Svozilík, J. P. Torres, and A. B. U'ren, "Temperature-controlled entangled-photon absorption spectroscopy," Phys. Rev. Lett. **123**, 023601 (2019).
20. S. Mukamel, M. Freyberger, W. Schleich, M. Bellini, A. Zavatta, G. Leuchs, C. Silberhorn, R. W. Boyd, L. L. Sánchez-Soto, A. Stefanov, M. Barbieri, A. Paterova, L. Krivitsky, S. Shwartz, K. Tamasaku, K.

Dorfman, F. Schlawin, V. Sandoghdar, M. Raymer, A. Marcus, O. Varnavski, T. Goodson, Z.-Y. Zhou, B.-S. Shi, S. Asban, M. Scully, G. Agarwal, T. Peng, A. V. Sokolov, Z.-D. Zhang, M. S. Zubairy, I. A. Vartanyants, E. del Valle, and F. Laussy, "Roadmap on quantum light spectroscopy," J. Phys. B **53**, 072002 (2020).
21. M. G. Raymer, T. Landes, and A. H. Marcus, "Entangled two-photon absorption by atoms and molecules: a quantum optics tutorial," arXiv:2103.02551 (2021).
22. T. Landes, M. G. Raymer, M. Allgaier, S. Merkouche, B. J. Smith, and A. H. Marcus, "Quantifying the enhancement of two-photon absorption due to spectral-temporal entanglement," arXiv:2103.10530 (2021).
23. M. G. Raymer, T. Landes, M. Allgaier, S. Merkouche, B. J. Smith, and A. H. Marcus, "How large is the quantum enhancement of two-photon absorption by time-frequency entanglement of photon pairs?" Optica **8**, 757–758 (2021).
24. J. P. Villabona-Monsalve, R. K. Burdick, and T. Goodson, "Measurements of entangled two-photon absorption in organic molecules with CW-pumped type-i spontaneous parametric down-conversion," J. Phys. Chem. C **124**, 24526–24532 (2020).
25. K. M. Parzuchowski, A. Mikhaylov, M. D. Mazurek, R. N. Wilson, D. J. Lum, T. Gerrits, C. H. Camp, M. J. Stevens, and R. Jimenez, "Setting bounds on entangled two-photon absorption cross sections in common fluorophores," Phys. Rev. Appl. **15**, 044012 (2021).
26. D. Tabakaev, M. Montagnese, G. Haack, L. Bonacina, J.-P. Wolf, H. Zbinden, and R. T. Thew, "Energy-time-entangled two-photon molecular absorption," Phys. Rev. A **103**, 033701 (2021).
27. S. Corona-Aquino, O. Calderón-Losada, M. Y. Li-Gómez, H. Cruz-Ramírez, V. Alvarez-Venicio, M. P. Carreón-Castro, R. de J. León-Montiel, and A. B. U'ren, "Experimental study on the effects of photon-pair temporal correlations in entangled two-photon absorption," arXiv:2101.10987 (2021).
28. S. Lerch and A. Stefanov, "Experimental requirements for entangled two-photon spectroscopy," arXiv:2103.10079 (2021).
29. A. R. Guzman, M. R. Harpham, O. Süzer, M. M. Haley, and T. G. Goodson, "Spatial control of entangled two-photon absorption with organic chromophores," J. Am. Chem. Soc. **132**, 7840–7841 (2010).
30. F. Schlawin, K. Dorfman, B. Fingerhut, and S. Mukamel, "Suppression of population transport and control of exciton distributions by entangled photons," Nat. Commun. **4**, 1782 (2013).
31. H.-B. Fei, B. M. Jost, S. Popescu, B. E. A. Saleh, and M. C. Teich, "Entanglement-induced two-photon transparency," Phys. Rev. Lett. **78**, 1679–1682 (1997).
32. B. W. Shore, "Definition of virtual levels," Am. J. Phys. **47**, 262–263 (1979).
33. R. Walder, D. H. Paik, M. S. Bull, C. Sauer, and T. T. Perkins, "Ultrastable measurement platform: sub-nm drift over hours in 3D at room temperature," Opt. Express **23**, 16554–16564 (2015).
34. A. Fedrizzi, T. Herbst, M. Aspelmeyer, M. Barbieri, T. Jennewein, and A. Zeilinger, "Anti-symmetrization reveals hidden entanglement," New J. Phys. **11**, 103052 (2009).